On the Transient Radiation of Energy from Simple Current Distributions and Linear Antennas

Glenn S. Smith and Thorsten W. Hertel

School of Electrical and Computer Engineering, Georgia Institute of Technology
Atlanta, GA 30332-0250 USA
Tel: +1 (404) 894-2922; Fax: +1 (404) 894-4641; E-mail: glenn.smith@ece.gatech.edu; hertel@ieee.org

Keywords: Electromagnetic radiation; transient radiation; antenna theory; antenna transient analysis; current distribution; linear antennas

1. Introduction

During the last few years, a number of articles have appeared in the publications of this Society that deal with the radiation from simple filamentary current distributions and simple wire antennas [1-6]. The purpose of these articles generally is to add to the physical understanding of the process of radiation: that is, to add to the understanding of where radiation originates on these structures, and the mechanism by which energy propagates away from the structures to the far zone.

In an earlier article, we examined the radiation from two simple filamentary current distributions: traveling-wave and uniform [3]. The radiated or far-zone electric field was computed for an excitation that was a Gaussian pulse in time. Two interpretations for the origin of the radiation were presented, based on the far-field results. In this article, we continue this investigation; however, the emphasis is on an examination of the near field and the related transport of energy away from the current filament. In this article, we examine traveling-wave and standing-wave current distributions, because these distributions are frequently used to model practical antennas.

Exact analytical expressions are presented for the electric and magnetic fields of the assumed, filamentary current distributions when the excitation is a general function of time. For the filamentary distributions, the current and charge are confined to a line (a line source). There is no radius associated with the filament. The expressions for the fields apply in both the near and far zones, and are used to determine the Poynting vector. For an excitation that is a Gaussian pulse in time, exact analytical expressions are obtained for the energy leaving the filament per unit time per unit length, the total energy leaving the filament per unit length, and the total energy radiated. Graphical results based on these expressions are used to study the energy transport from the filamentary current distributions.

At the end of the article, the results for the standing-wave current distribution are compared with those from an accurate analysis of a pulse-excited, cylindrical monopole antenna, performed using the Finite-Difference Time-Domain (FDTD) method. This comparison shows how the energy transport for the assumed current distribution is related to that for an actual antenna.

2. Electromagnetic Fields of Two Filamentary Current Distributions

The geometry and the associated coordinates for the traveling-wave current distribution, which we call the *traveling-wave element*, are shown in Figure 1a. The element, of length h, is aligned with the z axis. There is a source of current $I_s(t)$ at the bottom of the element, and there is a perfect termination at the top of the element. A traveling wave of current leaves the source and propagates along the element at the speed of light, c, until it reaches the termination, where it is totally absorbed. The distribution for the axial current is

$$I(z,t) = I_s(t - z/c)\left[U(z) - U(z-h)\right], \tag{1}$$

and, from the equation of continuity for electric charge, the charge per unit length on the element is

$$Q(z,t) = Q_s(t - z/c)\left[U(z) - U(z-h)\right] + q_0(t)\delta(z) + q_h(t)\delta(z-h), \tag{2}$$

where

$$Q_s(t) = I_s(t)/c,$$

$$q_0(t) = -\int_{t'=-\infty}^{t} I_s(t')\,dt',$$

$$q_h(t) = \int_{t'=-\infty}^{t} I_s(t' - h/c)\,dt'. \tag{3}$$

Here, U is the Heaviside unit-step function, and δ is the Dirac delta function. The three terms in Equation (2) represent a traveling wave of positive charge, Q_s, propagating along the element at the speed of light; a negative charge, q_0, that is left behind at the lower end as the pulse of positive charge leaves the source (the element is electrically neutral); and a positive charge, q_h, that accumulates at the upper end as the pulse enters the termination.

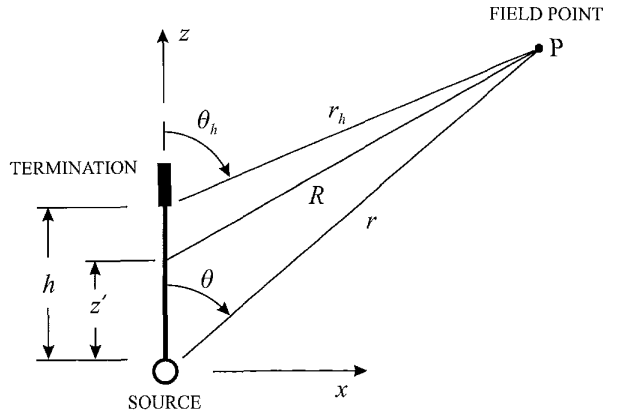

Figure 1a. A schematic drawing showing the traveling-wave element with the coordinates used in evaluating the electromagnetic field.

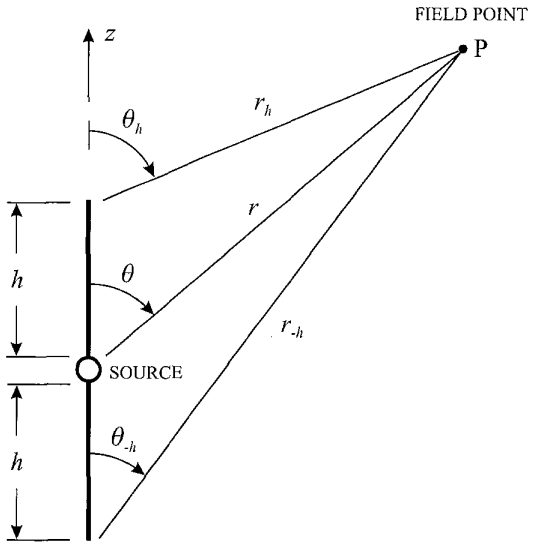

Figure 1b. A schematic drawing showing the standing-wave dipole with the coordinates used in evaluating the electromagnetic field.

The geometry and the associated coordinates for the standing-wave current distribution, which we call the *standing-wave dipole*, are shown in Figure 1b. This terminology is used because the distribution becomes the familiar standing wave when the excitation is time harmonic. It is a dipole with the arms (each of length h) aligned with the z axis. There is a source of current, $I_s(t)$, at the center of the dipole ($z=0$). The source produces a traveling wave of current (a pulse of positive charge) that propagates at the speed of light up the top arm of the dipole. A similar traveling wave of current (a pulse of negative charge) propagates down the bottom arm of the dipole. These waves are totally reflected when they reach the open ends of the dipole at time $t=\tau_a=h/c$. This produces traveling waves of current that propagate on the arms from the open ends toward the source. These waves are totally absorbed when they reach the source at time $t=2\tau_a=2h/c$. The distribution for the axial current is

$$I(z,t)=\left[I_s(t-z/c)-I_s(t+z/c-2h/c)\right]\left[U(z)-U(z-h)\right]+\left[I_s(t+z/c)-I_s(t-z/c-2h/c)\right]\left[U(z+h)-U(z)\right], \tag{4}$$

and the charge per unit length on the dipole is

$$Q(z,t)=\left[Q_s(t-z/c)+Q_s(t+z/c-2h/c)\right]\left[U(z)-U(z-h)\right]-\left[Q_s(t+z/c)+Q_s(t-z/c-2h/c)\right]\left[U(z+h)-U(z)\right]. \tag{5}$$

As discussed in reference [7], the standing-wave dipole can be can be viewed as a combination of four basic traveling-wave elements. Two elements are arranged to produce outward-traveling waves on the arms, starting at time $t=0$, and two elements are arranged to produce inward-traveling waves, starting at time $t=\tau_a=h/c$. This representation is easily understood by comparing the current distributions given in Equations (1) and (4): Equation (4) is the sum of four terms, each with the same form as Equation (1). Notice from Equation (5) that there is no accumulation of charge at the center or ends of the standing-wave dipole as there is for the traveling-wave element of Equation (2). For the standing-wave dipole, equal amounts of positive and negative charge simultaneously leave or enter the source, and the traveling waves of charge are totally reflected at the open ends.

The complete electromagnetic field (both the near field and far field) of these current distributions can be obtained in closed form. The derivation is presented in reference [8], so only the final results will be given here. The field for the traveling-wave element is

$$\vec{E}(\vec{r},t)=\frac{1}{4\pi\varepsilon_0}\left[\frac{q_0(t-r/c)}{r^2}\hat{r}+\frac{q_h(t-r_h/c)}{r_h^2}\hat{r}_h+\frac{\cot(\theta/2)I_s(t-r/c)}{cr}\hat{\theta}-\frac{\cot(\theta_h/2)I_s(t-h/c-r_h/c)}{cr_h}\hat{\theta}_h\right], \tag{6}$$

$$\vec{B}(\vec{r},t)=\frac{\mu_0}{4\pi}\left[\frac{\cot(\theta/2)I_s(t-r/c)}{r}-\frac{\cot(\theta_h/2)I_s(t-h/c-r_h/c)}{r_h}\right]\hat{\varphi}, \tag{7}$$

and the field for the standing-wave dipole is

$$\vec{E}(\vec{r},t)=\frac{\mu_0 c}{2\pi r\sin\theta}\left\{\left[I_s(t-r/c)+I_s(t-2h/c-r/c)\right]\hat{\theta}-I_s(t-h/c-r_h/c)\,\hat{\theta}_h-I_s(t-h/c-r_{-h}/c)\,\hat{\theta}_{-h}\right\}, \tag{8}$$

$$\vec{B}(\vec{r},t)=\frac{\mu_0}{2\pi r\sin\theta}\left[I_s(t-r/c)+I_s(t-2h/c-r/c)-I_s(t-h/c-r_h/c)-I_s(t-h/c-r_{-h}/c)\right]\hat{\varphi}. \tag{9}$$

There are three spherical coordinate systems used in the description of these fields: they are shown in Figure 1. For the standing-wave dipole, they are the system r,θ,φ, with origin at the center of the dipole; the system r_h,θ_h,φ_h, with origin at the top of the dipole; and the system $r_{-h},\theta_{-h},\varphi_{-h}$, with origin at the bottom of the dipole. The azimuthal coordinate is the same in all systems, so $\hat{\varphi}_h=\hat{\varphi}_{-h}=\hat{\varphi}$.

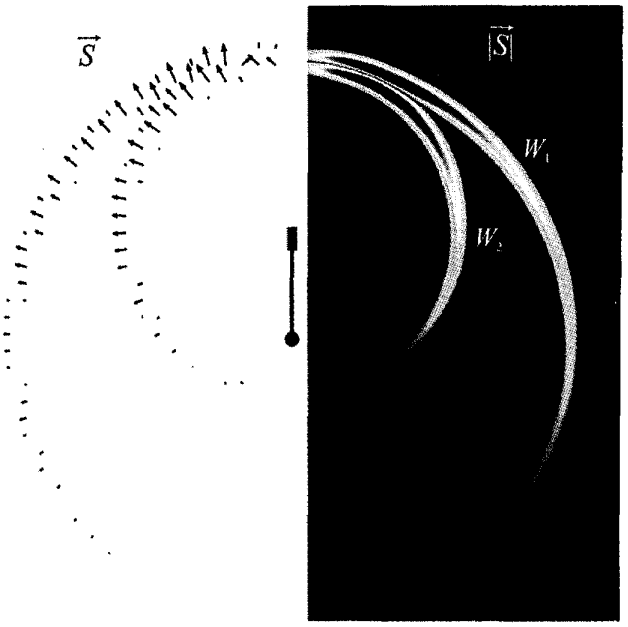

Figure 2. A plot of the Poynting vector for the traveling-wave element at the time $t/\tau_a = 2.5$: the right side is the magnitude, the left side shows the vectors. Logarithmic scaling is used for both sides.

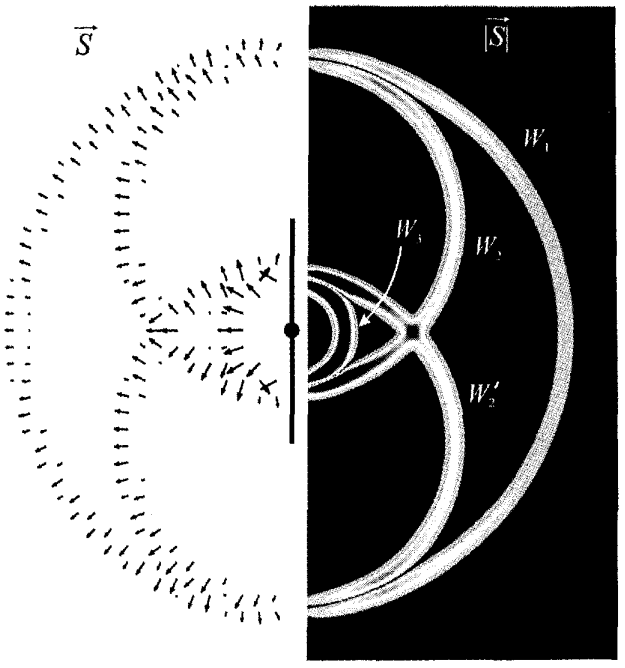

Figure 3. A plot of the Poynting vector for the standing-wave dipole at the time $t/\tau_a = 2.5$: the right side is the magnitude, the left side shows the vectors. Logarithmic scaling is used for both sides.

In the limit as $r \to \infty$, Equations (6)-(9) simplify to become the radiated or far-zone field [7, 8]. For the traveling-wave element, the electric field is

$$\vec{E}^r(r,t) = \frac{\mu_0 c \sin\theta}{4\pi r(1-\cos\theta)}\{I_s(t-r/c) - I_s[t-r/c-(h/c)(1-\cos\theta)]\}\hat{\theta}, \quad (10)$$

and for the standing-wave dipole, the electric field is

$$\vec{E}^r(\vec{r},t) = \frac{\mu_0 c}{2\pi r\sin\theta}\{I_s(t-r/c)+I_s(t-r/c-2h/c) - I_s[t-r/c-(h/c)(1-\cos\theta)]-I_s[t-r/c-(h/c)(1+\cos\theta)]\}\hat{\theta}. \quad (11)$$

For both distributions, the radiated magnetic field is simply

$$\vec{B}^r(\vec{r},t) = \frac{1}{c}\hat{r}\times\vec{E}^r(\vec{r},t). \quad (12)$$

Notice that the superscript r is used to indicate the radiated or far-zone field.

In the calculations that follow, the current of the source is assumed to be a Gaussian pulse of the form

$$I_s(t) = I_0 e^{-(t/\tau)^2}, \quad (13)$$

where τ is the characteristic time. For all numerical results, we will use $\tau/\tau_a = 0.076$; then, the width of the pulse in space is approximately one fourth of the length of an element (four pulses fit along the length h).

The expressions for the electric and magnetic fields of the current distributions, Equations (6)-(9), apply at any point not directly on the filament. Therefore, we can use these expressions to calculate the Poynting vector in the space surrounding the filament:

$$\vec{S}(\vec{r},t) = \frac{1}{\mu_0}\vec{E}(\vec{r},t)\times\vec{B}(\vec{r},t). \quad (14)$$

Figures 2 and 3 show the Poynting vector for the field of the traveling-wave element and of the standing-wave dipole, respectively, at the time $t/\tau_a = 2.5$. In these figures, the Poynting vector is not plotted within a narrow region adjacent to the filaments, specifically, for $\rho < 0.15h$, where ρ is the radial distance from the filament, because – as we will show later – the Poynting vector becomes infinite at the filaments. On the right-hand side of these figures, the logarithm of the magnitude of the Poynting vector, $|\vec{S}|$, is plotted on a color scale. The intensity of the field increases as the hue goes from blue to red, and the range for the values of $|\vec{S}|$ displayed is $10^4:1$. On the left-hand side of these figures, the arrows indicate the direction of the Poynting vector, and the length of an arrow is proportional to the logarithm of $|\vec{S}|$.

For the traveling-wave element, a spherical wavefront, W_1, centered at $z=0$, is produced when the pulse leaves the source, and a second spherical wavefront, W_2, centered at $z=h$, is produced when the pulse is absorbed by the termination. These wavefronts travel outward from the ends of the element at the speed of light. For the standing-wave dipole, there are four spherical wavefronts: W_1, centered at $z=0$, is produced when the pulses leave the source; W_2 and W_2', centered at $z=h$ and $z=-h$, respectively, are produced when the pulses are reflected from the open ends; and W_3, centered at $z=0$, is produced when the pulses are absorbed at the source. For all of the wavefronts, the Poynting vectors are seen to be predominantly normal to the wavefront. Notice that the energy is not distributed uniformly over a spherical wavefront, but is concentrated in certain regions. This can be clearly seen in Figure 2 for the traveling-wave element, where the concentration of energy is highest for wavefronts W_1 and W_2 within the red areas at the angle $\theta \approx 20°$.

It is not surprising that the graphical results in Figures 2 and 3 show spherical wavefronts centered on the source and ends of the filaments, for the formulas for the electromagnetic field, Equations (6)-(9), directly support this interpretation. Consider the formula for the electric field of the traveling-wave element of Equation (6). The first and third terms in this formula involve only the radial distance, r, from the source (not r_h), and the time delay, $t-r/c$. Thus, these terms can be interpreted as spherical waves centered on the source, $z=0$. The second and fourth terms in this formula involve only the radial distance, r_h, from the termination (not r), and the time delay, $t-r_h/c$ or $t-h/c-r_h/c$. Thus, these terms can be interpreted as spherical waves centered on the termination, $z=h$. A similar argument can be used with the formula for the electric field of the standing-wave dipole, Equation (8), once one recognizes that $r\sin\theta = r_h\sin\theta_h = r_{-h}\sin\theta_{-h}$.

3. Total Energy Radiated by the Filamentary Current Distributions

The total energy radiated by a filament is determined by integrating the normal component of the Poynting vector for the radiated field, $\vec{S}^r$, over the surface of a large sphere surrounding the filament and over all time:

$$U_{\text{rad}} = 2\pi\int_{t=-\infty}^{\infty}\int_{\theta=0}^{\pi}\hat{r}\cdot\vec{S}^r r^2\sin\theta\,d\theta\,dt = \frac{2\pi}{\zeta_0}\int_{t=-\infty}^{\infty}\int_{\theta=0}^{\pi}\left|\vec{E}^r\right|^2 r^2\sin\theta\,d\theta\,dt \quad (15)$$

where $\zeta_0 = \sqrt{\mu_0/\varepsilon_0}$ is the wave impedance of free space. Surprisingly, this expression can be evaluated in closed form for both current distributions when the source current is the Gaussian pulse of Equation (13) (see Appendix A). For the traveling-wave element, we obtain

$$U_{\text{rad}} = \frac{\zeta_0\tau I_0^2}{4\sqrt{2\pi}}\left\{\gamma - 2 + \ln\left[2(\tau_a/\tau)^2\right] + \sqrt{\frac{\pi}{2}}\left(\frac{\tau}{\tau_a}\right)\text{erf}\left[\sqrt{2}(\tau_a/\tau)\right] + \text{E}_1\left[2(\tau_a/\tau)^2\right]\right\}, \quad (16)$$

and for the standing-wave dipole

$$U_{\text{rad}} = \frac{\zeta_0\tau I_0^2}{\sqrt{2\pi}}\left(\left\{\gamma + \ln\left[2(\tau_a/\tau)^2\right]\right\}\left\{1+\exp\left[-2(\tau_a/\tau)^2\right]\right\} + \text{E}_1\left[2(\tau_a/\tau)^2\right] - \exp\left[-2(\tau_a/\tau)^2\right]\text{Ei}\left[2(\tau_a/\tau)^2\right]\right). \quad (17)$$

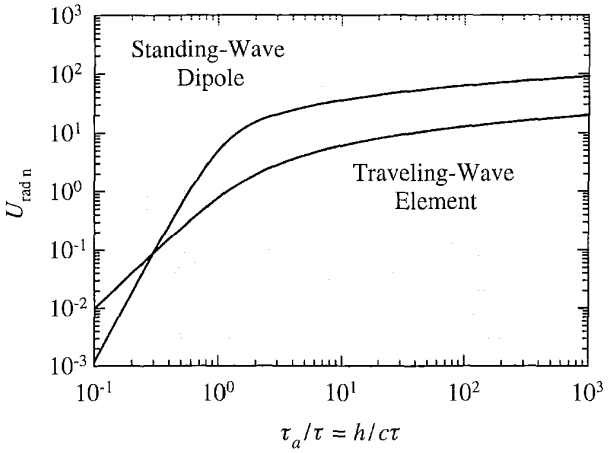

Figure 4. The total energy radiated by filaments excited by a Gaussian pulse of characteristic time τ, $\tau_a = h/c$.

Here, $\gamma = 0.57721...$ is Euler's constant, erf is the error function, and E_1 and Ei are exponential integrals [9].

In Figure 4, the total energy radiated is plotted in normalized form,

$$U_{\text{rad n}} = U_{\text{rad}} \Big/ \left(\frac{\zeta_o \tau I_o^2}{6\sqrt{2\pi}} \right), \tag{18}$$

versus the parameter $\tau_a/\tau = h/c\tau$, which is the time for light to travel the length h divided by the characteristic time for the pulse. For both distributions, traveling-wave and standing-wave, the total energy radiated is seen to increase monotonically with increasing τ_a/τ (with increasing length of the element or dipole). This behavior is easily explained. Consider the spherical wavefront W_1 for the traveling-wave element, shown in Figure 2. This wavefront originated at the source end of the element. As the wavefront expanded, it stayed in contact with the element for the length of time τ_a. During this time, energy continually left the element and entered the wavefront (this will be shown explicitly in the next section, Figure 6). Hence, an increase in τ_a/τ causes an increase in the energy within the wavefront and an increase in the total energy radiated.

When the filaments are electrically short, that is, in the limit $\tau_a/\tau \to 0$, the energies are

$$U_{\text{rad n}} \sim (\tau_a/\tau)^2, \text{ traveling-wave element,} \tag{19}$$

$$U_{\text{rad n}} \sim 12(\tau_a/\tau)^4, \text{ standing-wave dipole.} \tag{20}$$

Notice that these energies differ by a factor of $(\tau_a/\tau)^2$. This difference is explained when we recall the relationship between the Poynting vector of the radiated field, which appears in Equation (15), and the electric dipole moment, p, of these electrically short filaments [7]:

$$|\vec{S}^r| \propto \left(\frac{d^2 p}{dt^2} \right)^2 \propto \left[h \frac{dI(z=0,t)}{dt} \right]^2 \propto \left(\frac{\tau_a}{\tau} \right)^2 \left[\frac{dI(z=0,t)}{d(t/\tau)} \right]^2 \tag{21}$$

So, for the traveling-wave element with the current of Equation (1), we have

$$|\vec{S}^r| \propto \left(\frac{\tau_a}{\tau} \right)^2 \left[\frac{dI_s(t)}{d(t/\tau)} \right]^2, \tag{22}$$

and for the standing-wave dipole with the current of Equation (4), we have

$$\begin{aligned} |\vec{S}^r| &\propto 4\left(\frac{\tau_a}{\tau} \right)^2 \left[\frac{dI_s(t)}{d(t/\tau)} - \frac{dI_s(t-2h/c)}{d(t/\tau)} \right]^2 \\ &\approx 4\left(\frac{\tau_a}{\tau} \right)^2 \left[2\left(\frac{\tau_a}{\tau} \right) \frac{d^2 I_s(t)}{d(t/\tau)^2} \right]^2 \\ &\propto \left(\frac{\tau_a}{\tau} \right)^4 \left[\frac{d^2 I_s(t)}{d(t/\tau)^2} \right]^2, \end{aligned} \tag{23}$$

which, in agreement with Equations (19) and (20), differ by a factor of $(\tau_a/\tau)^2$.

When the filaments are electrically long, that is, in the limit $\tau_a/\tau \to \infty$, the energies are

$$U_{\text{rad n}} \sim 3\ln(\tau_a/\tau), \text{ traveling-wave,} \tag{24}$$

$$U_{\text{rad n}} \sim 12\ln(\tau_a/\tau), \text{ standing-wave.} \tag{25}$$

Notice that these energies differ by a factor of four. To explain this difference, we will first consider the plot in Figure 2 for the Poynting vector of the traveling-wave element. As mentioned earlier, for wavefronts W_1 and W_2, the concentration of energy is highest within the red areas at the angle $\theta \approx 20°$. As the length of the element is made longer (as τ_a/τ is increased), the energy within these regions increases, and the regions move closer to the z axis (to a smaller angle θ). This effect is probably more familiar for traveling-wave antennas with time-harmonic excitation, where the main lobe in the far-field pattern decreases in width and moves to a smaller angle as the electrical length of the antenna is increased [7]. For a long element, these regions contain most of the energy radiated by the element. Now, there are four times as many regions like this for the standing-wave dipole as there are for the traveling-wave element. For the standing-wave dipole, shown in Figure 3, these regions occur where the following wavefronts overlap: W_1 and W_2, W_1 and W_2', W_2 and W_3, and W_2' and W_3. (This is more easily seen in plots for a longer time, t/τ_a, than shown in Figure 3, when all of the wavefronts have expanded beyond the dipole.) Therefore, the energy radiated by the standing-wave dipole is approximately four times that radiated by the traveling-wave element.

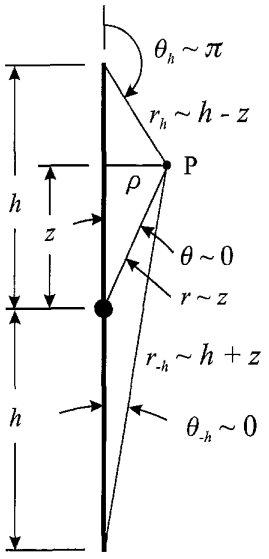

Figure 5. The coordinates for a point P close to the filament of current, $\rho \ll h$, $0 < z < h$.

4. Transport of Energy Away from the Filamentary Current Distributions

Using plots of the Poynting vector, we can examine the transport of energy very close to the filament of current. For this analysis, we will express the Poynting vector, Equation (14), in terms of the circular cylindrical coordinates ρ, φ, z, centered at the source:

$$\vec{S} = S_\rho \hat{\rho} + S_z \hat{z} = \frac{1}{\mu_o}\left(-E_z B_\varphi \hat{\rho} + E_\rho B_\varphi \hat{z}\right). \tag{26}$$

First, we will consider the radial component of the Poynting vector, S_ρ, in the limit as $\rho \to 0$. This will be used to determine the energy leaving the filament per unit time per unit length:

$$\frac{dU}{dtdz} = \lim_{\rho \to 0}\left(2\pi\rho S_\rho\right). \tag{27}$$

To evaluate this expression, we must obtain asymptotic forms that apply in the limit $\rho \to 0$ for the distances, angles, and unit vectors that appear in the expressions for the components of the field, Equations (6)-(9). For a point z within the range $0 < z < h$ (see Figure 5), these forms are

$$\begin{aligned}
&r \sim z, && \theta \sim 0,\\
&\hat{r} \sim (\rho/z)\hat{\rho} + \hat{z}, && \hat{\theta} \sim \hat{\rho} - (\rho/z)\hat{z},\\
&r_h \sim h - z, && \theta_h \sim \pi,\\
&\hat{r}_h \sim \left[\rho/(h-z)\right]\hat{\rho} - \hat{z}, && \hat{\theta}_h \sim -\hat{\rho} - \left[\rho/(h-z)\right]\hat{z},\\
&r_{-h} \sim h + z, && \theta_{-h} \sim 0,\\
&\hat{r}_{-h} \sim \left[\rho/(h+z)\right]\hat{\rho} + \hat{z}, && \hat{\theta}_{-h} \sim \hat{\rho} - \left[\rho/(h+z)\right]\hat{z}.
\end{aligned} \tag{28}$$

When these results are substituted into the expressions for the field, the Poynting vector is evaluated, and the limit is taken, Equation (27) becomes, for the traveling-wave element,

$$\frac{dU}{dtdz} = \frac{\zeta_0}{4\pi}\left\{\frac{2\left[I_s(t-z/c)\right]^2}{z} - \frac{cI_s(t-z/c)q_0(t-z/c)}{z^2} + \frac{cI_s(t-z/c)q_h(t-h/c+z/c)}{(h-z)^2}\right\}, \tag{29}$$

and for the standing-wave dipole

$$\begin{aligned}
\frac{dU}{dtdz} = \frac{\zeta_0}{2\pi}\Bigg\{&\frac{\left[I_s(t-z/c)\right]^2}{z} + \frac{\left[I_s(t-2h/c+z/c)\right]^2}{h-z}\\
&- \frac{hI_s(t-z/c)I_s(t-2h/c+z/c)}{z(h-z)}\\
&+ \frac{hI_s(t-2h/c-z/c)\left[I_s(t-z/c) - I_s(t-2h/c+z/c)\right]}{z(h+z)}\Bigg\}.
\end{aligned} \tag{30}$$

In Equation (30), we have given the result for the top half of the dipole; by symmetry, the result for the bottom half is the same. Outside of the region for which Equations (29) and (30) apply – that is, for $z/h < 0$, $z/h > 1$ for the traveling-wave element, and for $|z/h| > 1$ for the standing-wave dipole – a detailed analysis shows that $dU/dtdz = 0$.

For the special case where the current of the source is the Gaussian pulse, Equation (13), these expressions become the following: for the traveling-wave element,

$$\begin{aligned}
\left(\frac{dU}{dtdz}\right)\left(\frac{h\tau}{U_{\text{rad}}}\right) = \frac{6}{\sqrt{2\pi}U_{\text{rad n}}}\Bigg[&\frac{\exp\left\{-2\left[(t_n - z_n)(\tau_a/\tau)\right]^2\right\}}{z_n}\\
&+ \frac{\sqrt{\pi}}{4}\left(\frac{\tau}{\tau_a}\right)\exp\left\{-\left[(t_n - z_n)(\tau_a/\tau)\right]^2\right\}\\
&\times\left(\frac{1}{z_n^2}\left\{1 + \operatorname{erf}\left[(t_n - z_n)(\tau_a/\tau)\right]\right\}\right.\\
&\left.+ \frac{1}{(1-z_n)^2}\left\{1 + \operatorname{erf}\left[(t_n + z_n - 2)(\tau_a/\tau)\right]\right\}\right)\Bigg],
\end{aligned} \tag{31}$$

and for the standing-wave dipole,

$$\begin{aligned}
\left(\frac{dU}{dtdz}\right)\left(\frac{2h\tau}{U_{\text{rad}}}\right) = \frac{12}{\sqrt{2\pi}U_{\text{rad n}}}\Bigg[&\frac{\exp\left\{-2\left[(t_n - z_n)(\tau_a/\tau)\right]^2\right\}}{z_n}\\
&+ \frac{\exp\left\{-2\left[(t_n - 2 + z_n)(\tau_a/\tau)\right]^2\right\}}{1-z_n}\\
&- \frac{\exp\left\{-\left[(t_n - z_n)(\tau_a/\tau)\right]^2\right\}\exp\left\{-\left[(t_n - 2 + z_n)(\tau_a/\tau)\right]^2\right\}}{z_n(1-z_n)}\\
&+ \frac{\exp\left\{-\left[(t_n - 2 - z_n)(\tau_a/\tau)\right]^2\right\}}{z_n(1+z_n)}\left(\exp\left\{-\left[(t_n - z_n)(\tau_a/\tau)\right]^2\right\}\right.
\end{aligned} \tag{32}$$

$$-\exp\left\{-\left[(t_n-2+z_n)(\tau_a/\tau)\right]^2\right\}\Big)\Big].$$

Here, to produce a dimensionless quantity, we have normalized the result by dividing by the total energy radiated by the filament, U_{rad}, divided by the length of the filament, h ($2h$ for the dipole), times the characteristic time for the pulse, τ. The normalized position $z_n = z/h$ and the normalized time $t_n = t/\tau_a = ct/h$ have also been introduced.

The total energy leaving a unit length of the filament is obtained by integrating Equation (27) over all time:

$$\frac{dU}{dz} = \int_{-\infty}^{\infty} \frac{dU}{dtdz}\,dt = \int_{-\infty}^{\infty} \lim_{\rho\to 0}\left(2\pi\rho S_\rho\right)dt. \tag{33}$$

When Equations (31) and (32) are substituted into this expression, a number of complicated integrals result, all of which can be evaluated in closed form (see Appendix B). We obtain for the traveling-wave element,

$$\left(\frac{dU}{dz}\right)\left(\frac{h}{U_{\text{rad}}}\right) = \frac{3}{U_{\text{rad n}}}\left[\frac{1}{z_n}+\frac{1}{2}\sqrt{\frac{\pi}{2}}\left(\frac{\tau}{\tau_a}\right)\right.$$
$$\left.\times\left(\frac{1}{z_n^2}+\frac{1}{(1-z_n)^2}\left\{1-\operatorname{erf}\left[\sqrt{2}\,(1-z_n)(\tau_a/\tau)\right]\right\}\right)\right], \tag{34}$$

and for the standing-wave dipole,

$$\left(\frac{dU}{dz}\right)\left(\frac{2h}{U_{\text{rad}}}\right) = \frac{6}{U_{\text{rad n}}}\left(\frac{1}{z_n(1-z_n)}\left\{1-\exp\left[-2(1-z_n)^2(\tau_a/\tau)^2\right]\right\}\right.$$
$$\left.+\frac{1}{z_n(1+z_n)}\left\{\exp\left[-2(\tau_a/\tau)^2\right]-\exp\left[-2z_n^2(\tau_a/\tau)^2\right]\right\}\right), \tag{35}$$

where, again, we have normalized the expression to produce a dimensionless quantity. We will now examine graphical results obtained from the four formulas: Equations (31), (32), and (34), (35).

4.1 Traveling-Wave Element

Figure 6 shows the normalized energy per unit time per unit length, Equation (31), leaving the element as a function of the normalized position, z/h, and the normalized time, t/τ_a. This graph is a series of one-dimensional plots (energy versus spatial position); each plot is for a fixed time. The plots are vertically displaced by an amount proportional to the time to show the progression of the signal along the element. Figure 7 shows the total normalized energy per unit length, Equation (34), leaving the element versus the normalized position, z/h.

From Figure 6, it is clear that as the pulse of current/charge moves along the element at the speed of light, energy leaves the element at the location of the pulse. Figure 7 shows that there is a net amount of energy leaving every unit length of the element. Initially, an infinite amount of energy leaves the source end of the element (point A in Figure 6). This supplies the infinite amount of energy stored in the field of the negative point charge q_0, Equation (3), that remains at the source end of the element. It also supplies the infinite amount of energy associated with the pulse of current/charge that travels up the element. A detailed calculation shows that when the pulse is out on the element, the axial component of the Poynting vector, S_z, very close to the element is approximately

$$S_z(\rho,z,t) \approx \frac{\zeta_0}{4\pi^2\rho^2}\left[I_s(t-z/c)\right]^2. \tag{36}$$

Thus, the energy per unit time passing through a small disc of radius ρ_0, centered on the filament, is

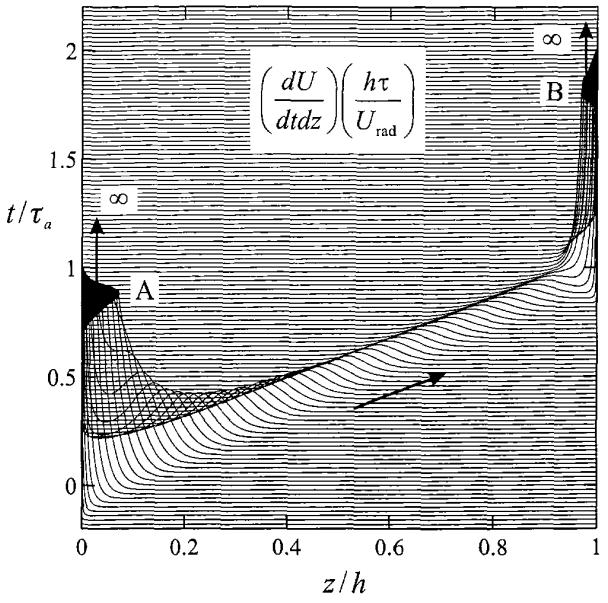

Figure 6. The energy per unit time per unit length leaving the traveling-wave element, $\tau/\tau_a = 0.076$.

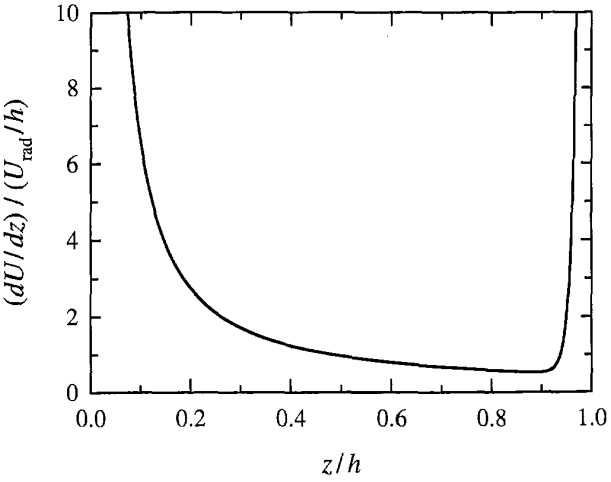

Figure 7. The total energy per unit length leaving the traveling-wave element, $\tau/\tau_a = 0.076$.

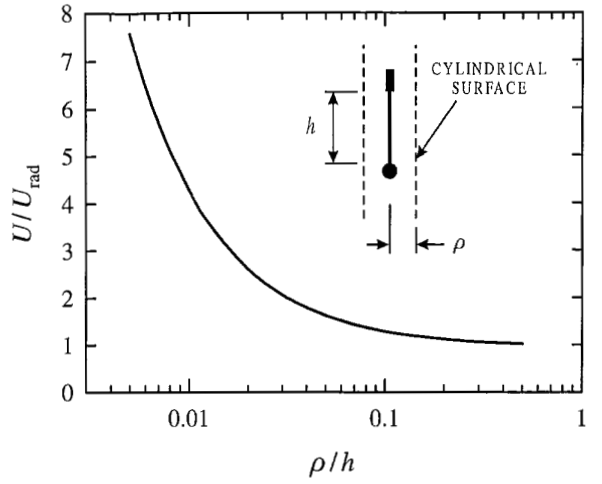

Figure 8a. The total energy leaving the cylindrical surface of radius ρ surrounding the traveling-wave element, $\tau/\tau_a = 0.076$.

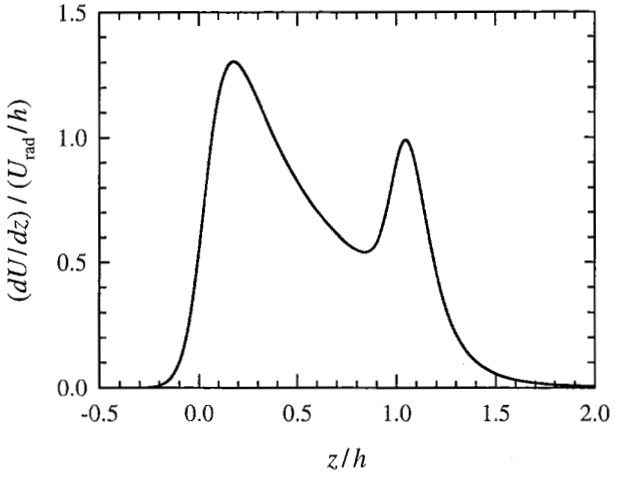

Figure 8b. The total energy per unit length leaving a cylinder of radius $\rho = 0.2h$ surrounding the traveling-wave element, $\tau/\tau_a = 0.076$.

$$\frac{dU}{dt} = 2\pi \int_{\rho=0}^{\rho_0} S_z \rho \, d\rho \approx \frac{\zeta_0}{2\pi}\left[I_s\left(t - z/c\right)\right]^2 \left[\ln(\rho)\right]_0^{\rho_0}, \quad (37)$$

which is clearly infinite. An infinite amount of energy also leaves the termination end of the element (point B in Figure 6). This supplies the infinite energy stored in the field of the positive point charge q_h, Equation (3), that remains at the termination end of the element.

The results in Figures 6 and 7 are for a cylindrical surface at the element, that is, for the limit $\rho \to 0$. Results for a cylindrical surface of any other radius surrounding the element can be obtained by numerically evaluating the expressions for the field, Equations (6) and (7), and the Poynting vector, Equation (26). In Figure 8a, we show the total energy passing through such a cylindrical surface, normalized to the total energy radiated, versus the normalized radius of the surface, ρ/h (see the inset in the figure for the geometry). As expected, the energy grows without bound as $\rho/h \to 0$. However, once $\rho/h > 0.2$, the energy passing through the surface is nearly constant and equal to the total energy radiated by the element. Figure 8b shows the energy per unit length passing through the surface with $\rho/h = 0.2$ versus the normalized position, z/h. The energy is spread out over a region that extends well beyond the ends of the element; however, there are well-defined peaks near the two ends. By inspection, we see that the area under this curve is approximately one, which is in agreement

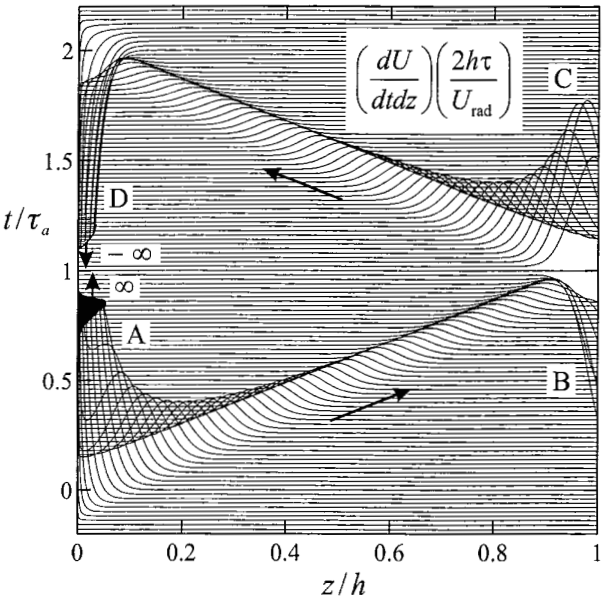

Figure 9. The energy per unit time per unit length leaving the standing-wave dipole, $\tau/\tau_a = 0.076$. The graph is for one half of the dipole; by symmetry, the result is the same for the other half.

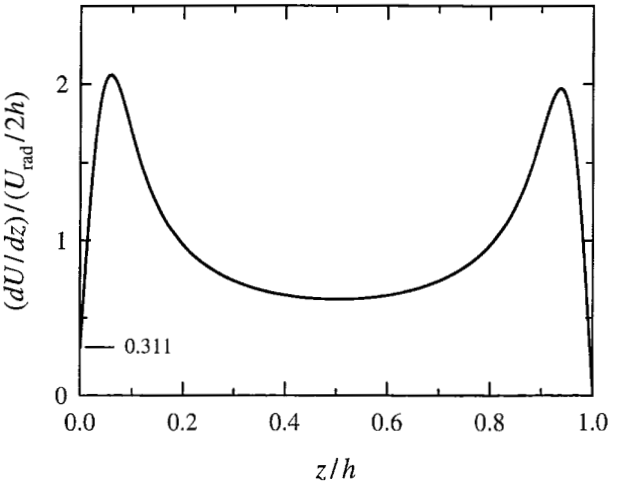

Figure 10. The total energy per unit length leaving the standing-wave dipole, $\tau/\tau_a = 0.076$. The graph is for one half of the dipole; by symmetry, the result is the same for the other half.

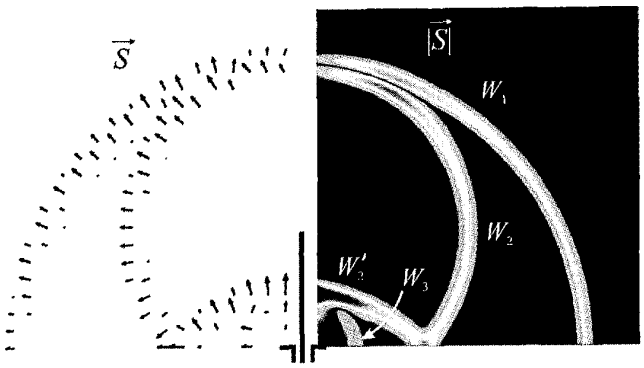

Figure 12. A plot of the Poynting vector for the cylindrical monopole antenna at the time $t/\tau_a = 2.5$: the right side is the magnitude, the left side shows the vectors. Logarithmic scaling is used for both sides.

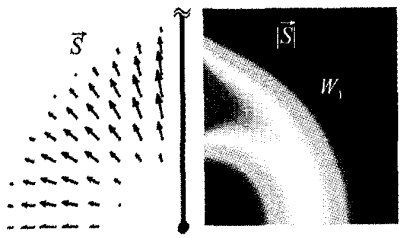

Figure 13a. A plot of the Poynting vector for the standing-wave dipole at the time $t/\tau_a = 0.3$: the right side is the magnitude, the left side shows the vectors. Logarithmic scaling is used for both sides.

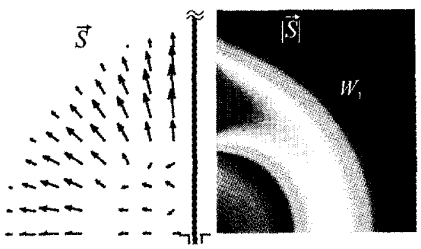

Figure 13b. A plot of the Poynting vector for the cylindrical monopole antenna at the time $t/\tau_a = 0.3$: the right side is the magnitude, the left side shows the vectors. Logarithmic scaling is used for both sides.

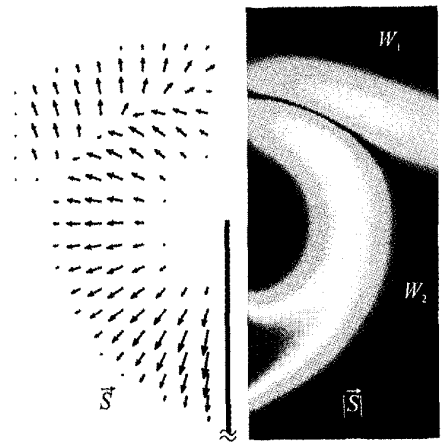

Figure 14a. A plot of the Poynting vector for the standing-wave dipole at the time $t/\tau_a = 1.3$: the right side is the magnitude, the left side shows the vectors. Logarithmic scaling is used for both sides.

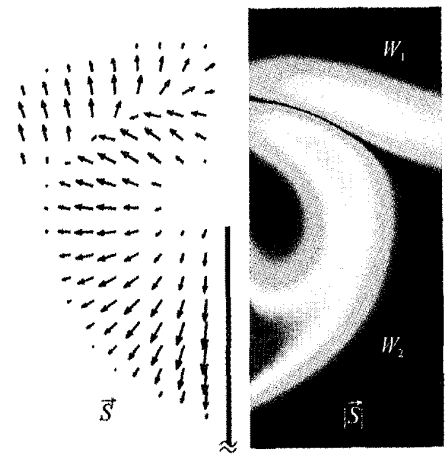

Figure 14b. A plot of the Poynting vector for the cylindrical monopole antenna at the time $t/\tau_a = 1.3$: the right side is the magnitude, the left side shows the vectors. Logarithmic scaling is used for both sides.

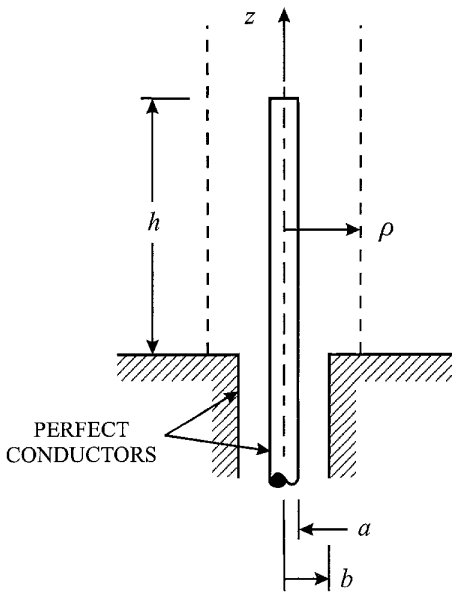

Figure 11. The geometry for the cylindrical monopole antenna.

with our earlier observation that practically all of the energy passing through a cylinder with this radius is radiated away.

4.2 Standing-Wave Dipole

Figures 9 and 10 show the normalized energy per unit time per unit length, Equation (32), and the total normalized energy per unit length, Equation (35), respectively, leaving the standing-wave dipole. These graphs are for the top half (arm) of the dipole; by symmetry, the results for the bottom half are the same. In Figure 9, we can clearly see that energy leaves/enters the arm of the dipole near the position of the pulse of current/charge as it travels along the arm. Initially, an infinite amount of energy leaves the source end of the arm (point A in Figure 9). This supplies the infinite amount of energy associated with the pulse of current/charge traveling along the arm, Equation (37). As the pulse approaches the open end of the arm ($z/h \approx 1$, $t/\tau_a \approx 1$), energy enters the arm (point B), and then as the pulse leaves the open end of the arm, energy leaves the arm (point C). When the pulse arrives at the source end of the arm ($z/h \approx 0$, $t/\tau_a \approx 2$), an infinite amount of energy enters the arm (point D). Figure 10 shows that there is a net amount of energy leaving every unit length of the arm, even though – as Figure 9 shows – at different times, energy can either leave or enter a particular point on the arm (points C and D).

At the point $z/h = 0$ in Figure 10, the energy per unit length appears to be zero, but it is not. A detailed calculation shows that it is

$$\left(\frac{dU}{dz}\right)_{z_n=0}\left(\frac{2h}{U_{\text{rad}}}\right) = \frac{12}{U_{\text{rad n}}}\left\{1-\exp\left[-2(\tau_a/\tau)^2\right]\left[2(\tau_a/\tau)^2+1\right]\right\}, \tag{38}$$

which has the numerical value 0.311... for the case shown in Figure 10.

For the standing-wave dipole, there is no point in making a graph of the total energy passing through a cylindrical surface surrounding the dipole, such as the graph shown in Figure 8a for the traveling-wave element. The graph would simply be a straight line of value 1.0, because, for the standing-wave dipole, the net energy passing through a cylinder of any radius is radiated away. Unlike the traveling-wave element, in the limit $t/\tau_a \to \infty$, no point charges remain at the ends of the arms of the standing-wave dipole; thus, there is no field around the dipole in which energy is stored.

The results presented above show that there is a net amount of energy leaving every unit length of both filamentary current distributions: the traveling-wave element and the standing-wave dipole. This energy must supply the energy stored in the near field of the filament, as well as the energy radiated to the far zone. It is not possible to say that energy leaving a particular point on the filament, such as an end, at a particular time contributes only to the radiated energy. For example, consider an amount of energy ΔU that leaves a unit length of the standing-wave dipole near the source ($z/h = 0$) at a time around $t/\tau_a = 0$. Several things could happen to this energy. It could contribute directly to the radiation. It could enter the field near the filament and travel along the filament until it reaches the open end ($z/h = 1$). At the open end, it could contribute to the radiation, it could be absorbed back into the filament, or it could travel down the filament toward the source.

5. Comparison with Results for a Cylindrical Monopole Antenna

The two filamentary current distributions discussed above are often used as approximate models for actual antennas. So a reasonable question to ask is, "How do the results for these models compare to those for actual antennas?" To answer this question, we will compare the results for the standing-wave dipole with those for a cylindrical monopole antenna. The results for the monopole antenna were calculated using the FDTD method. In the past, calculations made for the monopole antenna using this method were shown to be in excellent agreement with measurements [7, 10]. Therefore, we can safely assume that the results we calculate by this method are the same as what we would measure for an actual monopole antenna.

The cylindrical monopole antenna is shown in Figure 11. It is a vertical, perfectly conducting rod of radius a that extends a distance h above an infinite, perfectly conducting image plane. The monopole is fed through the image plane by a coaxial line. For the results to be presented, the radii of the inner and outer conductors of the line are $a = h/200$ [$\Omega = 2\ln(2h/a) \approx 12$] and $b = 2.30a$, and the incident voltage in the coaxial line is a Gaussian pulse with the same form as Equation (13):

$$V^i(t) = V_0 e^{-(t/\tau)^2}, \tag{39}$$

with $\tau/\tau_a = 0.076$.

Figure 12 shows the Poynting vector for the field of the monopole antenna at the time $t/\tau_a = 2.5$; this is to be compared with Figure 3 for the standing-wave dipole. The plots are very similar, and clearly show why this assumed current is often used to obtain a simple description for the radiation from the actual antenna. The most obvious difference in the plots occurs for the wavefront W_3 near the drive point, $z/h = 0$. This difference is due, in part, to the pulses in the assumed current being totally absorbed

when they reach the source at time $t/\tau_a \approx 2$. For the actual antenna, only a portion of the pulse of current enters the coaxial line (is absorbed), and the rest is reflected. The reflection of the pulses of current at the source can be included in the simple model, as shown in reference [7], and this would make the agreement with the FDTD results better. However, the inclusion of the reflection would unnecessarily complicate the calculations of the energy presented earlier: Equations (17), (32), and (35).

Additional comparisons of the Poynting vector of the assumed current (a standing-wave dipole) with that of the monopole antenna are in Figures 13 and 14. In these figures, the Poynting vector is not plotted within a narrow region adjacent to the filaments, specifically, for $\rho < 0.05h$. Figure 13 is for a time $t/\tau_a = 0.3$, when the pulse has just left the drive point, and Figure 14 is for a time $t/\tau_a = 1.3$, when the pulse has just been reflected from the open end. Again, we see that the two results are in good qualitative agreement. In both figures, the Poynting vectors are directed radially outward on a spherical surface, which indicates that energy is being transported away from both the drive point and the open end. Notice that there are differences in the distribution of energy within the colored rings. For example, in Figure 13, there is a circular, light-blue region near the drive point of the monopole and no similar region for the assumed current; and in Figure 14, close to the monopole the colored ring is wider for the monopole than for the assumed current. These differences are caused by dispersion (changes in shape) for the pulse of current as it leaves the coaxial line, travels along the monopole, and is reflected from the open end; there is no change in shape for the Gaussian pulse in the assumed current.

Despite the good qualitative agreement shown in these figures for the Poynting vectors for the assumed current (a standing-wave dipole) and the monopole antenna, we know that very close to these two structures the Poynting vectors must be very different. As can be seen in Figure 9, at every point along the standing-wave dipole there is a radial component of the Poynting vector at some time. For the perfectly conducting monopole, the radial component of the Poynting vector is always zero at the surface of the antenna, that is, at $\rho = a$. Stated differently, energy enters the space surrounding the standing-wave dipole at all points along its length, whereas energy enters the space surrounding the monopole antenna only through the coaxial aperture in the image plane. [One could interpret this result differently. One could say that there is energy entering and leaving the perfectly conducting monopole at every point on its surface. However, the energy entering is instantaneously equal to the energy leaving, so the net energy passing through the surface is zero.] To examine this point further, in Figure 15 we compare the total energy per unit length leaving the standing-wave dipole and the monopole.

The graphs in Figure 15 show dU/dz, appropriately normalized, versus z/h, for three cylindrical surfaces of different radius surrounding the structures: (a) $\rho/h = 0.0115$ $(\rho/b = 1.0)$, (b) $\rho/h = 0.115$ $(\rho/b = 10.0)$, and (c) $\rho/h = 0.230 (\rho/b = 20.0)$. The solid line is for the assumed current (a standing-wave dipole), and the dashed line is for the cylindrical monopole antenna. Notice that the vertical axis is logarithmically scaled. For the smallest radius, Figure 15a, the surface coincides with the outer conductor for the coaxial line of the monopole. For this case, the two distributions are very different. The large peak at $z/h = 0$ in the distribution for the monopole is caused by the energy leaving the coaxial aperture. Of course, there is no similar peak in the distribution for the assumed current. For the larger radii, Figures 15b and 15c, the dis-

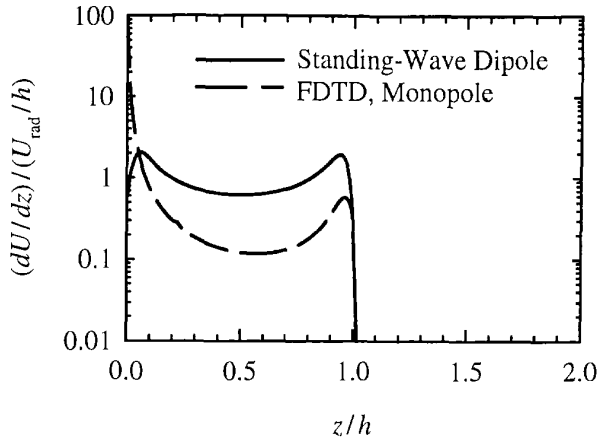

Figure 15a. The total energy per unit length leaving through a cylindrical surface of radius ρ surrounding the standing-wave dipole and the cylindrical monopole antenna, $\rho/h = 0.0115$.

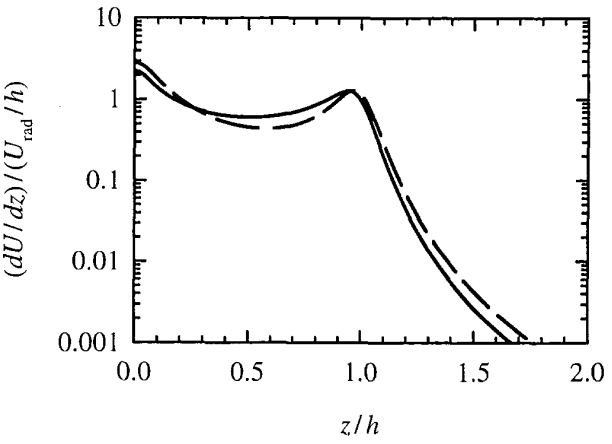

Figure 15b. The total energy per unit length leaving through a cylindrical surface of radius ρ surrounding the standing-wave dipole and the cylindrical monopole antenna, $\rho/h = 0.115$.

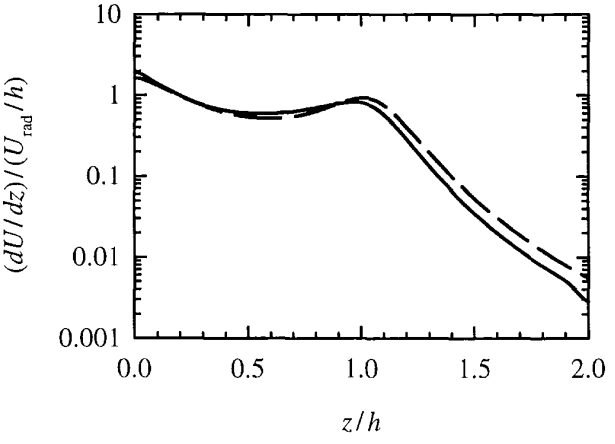

Figure 15c. The total energy per unit length leaving through a cylindrical surface of radius ρ surrounding the standing-wave dipole and the cylindrical monopole antenna, $\rho/h = 0.230$.

tributions for the two structures are very similar. So, we can conclude that even though energy leaves the surfaces of the two structures in completely different ways, once we are slightly away from the structures – at a radius that is typically 10% to 20% of the height of the monopole – the distribution of the energy in space is very similar for the two structures.

6. Discussion and Conclusions

In this paper, we considered the transient radiation from two simple, filamentary current distributions that are frequently used to model practical antennas: the traveling-wave element and the standing-wave dipole. Exact analytical expressions were presented for the electric and magnetic fields of these distributions when the excitation was a general function of time. These expressions apply in both the near and far zones. For an excitation that is a Gaussian pulse in time, exact analytical expressions were obtained for the energy leaving the filament per unit time per unit length, the total energy leaving the filament per unit length, and the total energy radiated. Graphical results based on these expressions were used to study the energy transported from the two filamentary current distributions. One interesting observation was that there is a net amount of energy leaving every unit length of both of these current distributions. For the traveling-wave element, some of this energy is radiated away from the element, and the rest is stored in the field of the point charges that remain at the two ends of the element. For the standing-wave dipole, this energy is all radiated away.

The results for the standing-wave dipole were compared with those from an accurate analysis of a cylindrical monopole antenna, performed using the FDTD method. The comparison showed the similarities as well as the differences in the energy transported from this simple filamentary current distribution and an actual antenna.

For the standing-wave dipole, a spherical wavefront, W_1 centered on the source, is produced as the pulse of current leaves the source ($t \approx 0$). As W_1 expands, it stays in contact with the filament and continually exchanges energy with the filament until it reaches the open end ($t \approx \tau_a$). Then, W_1 breaks away from the filament and expands into space. At the same time, a second spherical wavefront, W_2 (W_2'), centered on the open end, is also produced. As W_2 (W_2') expands, it stays in contact with the filament, and continually exchanges energy with the filament until it reaches the source ($t \approx 2\tau_a$). At this time, a third spherical wavefront, W_3, centered on the source, is also produced. After this time, both W_2 (W_2') and W_3 continue to expand. However, there is no further exchange of energy between these wavefronts and the filament, even though these wavefronts remain in contact with the filament until they reach the open ends ($t \approx 3\tau_a$), because there is no longer any current in the filament.

For the cylindrical monopole antenna, energy enters the space surrounding the antenna through the coaxial aperture when the incident voltage pulse reaches the end of the transmission line ($t \approx 0$). At this time, a spherical wavefront, W_1, centered on the aperture, is produced. As W_1 expands, it stays in contact with the monopole until it reaches the open end ($t \approx \tau_a$). It then breaks away from the monopole and expands into space. At the same time, a second spherical wavefront, W_2, centered on the open end, is also produced. W_2 expands until it encounters the image plane/aperture ($t \approx 2\tau_a$). At this time, some of this energy in W_2 enters the coaxial line where it is absorbed, and some of the energy in W_2 goes into the two new wavefronts, W_2' and W_3. This process goes on, with new wavefronts continually being produced, until all of the energy that initially left the coaxial aperture is carried away by the wavefronts or is absorbed back into the coaxial line.

There are several differences in the descriptions presented above for the energy transport very close to these two structures. Probably the most distinct difference is that energy is continually exchanged between the current filament and the spherical wavefronts as they travel along the filament, whereas no energy enters or leaves a spherical wavefront through the surface of the perfectly conducting monopole. Energy enters the space surrounding the antenna only through the coaxial aperture, and the perfectly conducting monopole simply serves to distribute this energy in space. Despite these differences, at a small distance from the structures (typically 10% to 20% of the length h) the energy transport is conspicuously similar. This is the reason that the simple model (a filamentary current) is useful for making good qualitative predictions for the radiation (far field) of the actual antenna (a monopole).

7. Acknowledgment

The authors would like to thank the reviewers for their comments. The senior author (GS) is grateful for the support provided by the John Pippin Chair in Electromagnetics that furthered this study. This research was supported in part by the Army Research Office under contract DAAG55-98-1-0403.

8. Appendix A

For the traveling-wave element, the total energy radiated, Equation (16), is obtained by substituting the expression for the radiated electric field, Equation (10), into Equation (15), and then replacing the current of the source by Equation (13):

$$U_{\text{rad}} = \frac{\zeta_0 I_0^2}{8\pi} \int_{t=-\infty}^{\infty} \int_{\theta=0}^{\pi} \Big[\exp\Big\{-2\big[(t-r/c)/\tau\big]^2\Big\} + \exp\Big(-2\big\{\big[t-r/c-\tau_a(1-\cos\theta)\big]/\tau\big\}^2\Big) - 2\exp\Big\{-\big[(t-r/c)/\tau\big]^2\Big\} \times \exp\Big(-\big\{\big[t-r/c-\tau_a(1-\cos\theta)\big]/\tau\big\}^2\Big)\Big] \frac{(\sin\theta)^3}{(1-\cos\theta)^2}\, d\theta dt. \tag{40}$$

After making the change of variable $\xi = (t-r/c)/\tau$ and completing the square in the exponent of the third term, Equation (40) becomes

$$U_{\text{rad}} = \frac{\zeta_0 \tau I_0^2}{8\pi} \int_{\xi=-\infty}^{\infty} \int_{\theta=0}^{\pi} \Big[\exp\big(-2\xi^2\big) + \exp\Big\{-2\big[\xi - (\tau_a/\tau)(1-\cos\theta)\big]^2\Big\} - 2\exp\Big[-1/2(\tau_a/\tau)^2(1-\cos\theta)^2\Big]$$

$$\times \exp\left\{-2\left[\xi - 1/2\,(\tau_a/\tau)(1-\cos\theta)\right]^2\right\}\Big] d\xi \frac{(\sin\theta)^3}{(1-\cos\theta)^2}\, d\theta$$

$$= \frac{\zeta_0 \tau I_0^2}{4\pi} \int_{\xi=-\infty}^{\infty} \exp\left(-2\xi^2\right) d\xi$$

$$\times \int_{\theta=0}^{\pi} \left\{ \frac{1 - \exp\left[-1/2\,(\tau_a/\tau)^2 (1-\cos\theta)^2\right]}{(1-\cos\theta)^2} \right\} (\sin\theta)^3\, d\theta$$

$$= \frac{\zeta_0 \tau I_0^2}{4\sqrt{2\pi}} \int_{\theta=0}^{\pi} \left\{ \frac{1 - \exp\left[-1/2\,(\tau_a/\tau)^2 (1-\cos\theta)^2\right]}{(1-\cos\theta)^2} \right\} (\sin\theta)^3\, d\theta . \tag{41}$$

Now, we will introduce the change of variable $\eta = (\tau_a/\tau)(1-\cos\theta)/\sqrt{2}$:

$$U_{\text{rad}} = \frac{\zeta_0 \tau I_0^2}{4\sqrt{2\pi}} \left\{ -\sqrt{2}\,(\tau/\tau_a) \int_0^{\sqrt{2}(\tau_a/\tau)} d\eta + \sqrt{2}\,(\tau/\tau_a) \right.$$

$$\left. \times \int_0^{\sqrt{2}(\tau_a/\tau)} \exp\left(-\eta^2\right) d\eta + 2 \int_0^{\sqrt{2}(\tau_a/\tau)} \left[\frac{1 - \exp\left(-\eta^2\right)}{\eta} \right] d\eta \right\}. \tag{42}$$

After evaluating the first integral and introducing the change of variable $\chi = \eta^2$ in the third integral, we obtain

$$U_{\text{rad}} = \frac{\zeta_0 \tau I_0^2}{4\sqrt{2\pi}} \left\{ -2 + \sqrt{2}\,(\tau/\tau_a) \int_0^{\sqrt{2}(\tau_a/\tau)} \exp\left(-\eta^2\right) d\eta \right.$$

$$\left. + \int_0^{2(\tau_a/\tau)^2} \left[\frac{1 - \exp(-\chi)}{\chi} \right] d\chi \right\}. \tag{43}$$

The integrals that remain are standard integrals, so our final answer is

$$U_{\text{rad}} = \frac{\zeta_0 \tau I_0^2}{4\sqrt{2\pi}} \left\{ \gamma - 2 + \ln\left[2\,(\tau_a/\tau)^2\right] \right.$$

$$\left. + \sqrt{\frac{\pi}{2}} \left(\frac{\tau}{\tau_a}\right) \operatorname{erf}\left[\sqrt{2}\,(\tau_a/\tau)\right] + \mathrm{E}_1\left[2\,(\tau_a/\tau)^2\right] \right\}, \tag{44}$$

where $\gamma = 0.57721...$ is Euler's constant, erf is the error function, and E_1 is an exponential integral [9].

The calculation for the total energy radiated by the standing-wave dipole, Equation (17), is more complicated: it involves ten double integrals, whereas this calculation only involved three double integrals. The procedures used, however, are similar to those used in this calculation.

9. Appendix B

For the traveling-wave element, the energy leaving a unit length of the element Equation (34) is obtained by substituting Equation (31) into Equation (33):

$$\left(\frac{dU}{dz}\right)\left(\frac{h}{U_{\text{rad}}}\right) =$$

$$\frac{6}{\sqrt{2\pi}\, U_{\text{rad n}}} \left(\frac{\tau_a}{\tau}\right) \left[\frac{1}{z_n} \int_{t_n=-\infty}^{\infty} \exp\left\{-2\left[(t_n - z_n)(\tau_a/\tau)\right]^2\right\} dt_n \right.$$

$$+ \frac{\sqrt{\pi}}{4} \left(\frac{\tau}{\tau_a}\right) \frac{1}{z_n^2} \int_{t_n=-\infty}^{\infty} \exp\left\{-\left[(t_n - z_n)(\tau_a/\tau)\right]^2\right\}$$

$$\times \left\{1 + \operatorname{erf}\left[(t_n - z_n)(\tau_a/\tau)\right]\right\} dt_n$$

$$+ \frac{\sqrt{\pi}}{4} \left(\frac{\tau}{\tau_a}\right) \frac{1}{(1-z_n)^2} \int_{t_n=-\infty}^{\infty} \exp\left\{-\left[(t_n - z_n)(\tau_a/\tau)\right]^2\right\}$$

$$\left. \times \left\{1 + \operatorname{erf}\left[(t_n + z_n - 2)(\tau_a/\tau)\right]\right\} dt_n \right]. \tag{45}$$

After making the change of variable $\xi = (t_n - z_n)(\tau_a/\tau)$ and writing out the error function,

$$1 + \operatorname{erf}(z) = \frac{2}{\sqrt{\pi}} \int_{\chi=-\infty}^{z} e^{-\chi^2} d\chi , \tag{46}$$

Equation (45) becomes

$$\left(\frac{dU}{dz}\right)\left(\frac{h}{U_{\text{rad}}}\right) = \frac{6}{\sqrt{2\pi}\, U_{\text{rad n}}} \left[\frac{1}{z_n} \int_{\xi=-\infty}^{\infty} e^{-2\xi^2} d\xi \right.$$

$$+ \frac{1}{2} \left(\frac{\tau}{\tau_a}\right) \frac{1}{z_n^2} \int_{\xi=-\infty}^{\infty} e^{-\xi^2} \int_{\chi=-\infty}^{\xi} e^{-\chi^2} d\chi\, d\xi$$

$$\left. + \frac{1}{2} \left(\frac{\tau}{\tau_a}\right) \frac{1}{(1-z_n)^2} \int_{\xi=-\infty}^{\infty} e^{-\xi^2} \int_{\chi=-\infty}^{\xi - 2(1-z_n)(\tau_a/\tau)} e^{-\chi^2} d\chi d\xi \right]. \tag{47}$$

Now, the first integral in Equation (47) has the value $\sqrt{\pi/2}$, and using integration by parts, we can show that the second integral has the value

$$\int_{\xi=-\infty}^{\infty} e^{-\xi^2} \int_{\chi=-\infty}^{\xi} e^{-\chi^2} d\chi d\xi = \frac{1}{2} \left[\int_{\chi=-\infty}^{\infty} e^{-\chi^2} d\chi \right]^2 = \frac{\pi}{2}. \tag{48}$$

To evaluate the third integral in Equation (47), we first introduce the change of variable $\eta = \chi - \left[\xi - 2(1-z_n)(\tau_a/\tau)\right]$, and then we interchange the order of the integrations to obtain

$$\int_{\xi=-\infty}^{\infty} e^{-\xi^2} \int_{\chi=-\infty}^{\xi - 2(1-z_n)(\tau_a/\tau)} e^{-\chi^2} d\chi d\xi$$

$$= \int_{\eta=-\infty}^{0} \int_{\xi=-\infty}^{\infty} \exp\left[-\left\{\eta+\left[\xi-2(1-z_n)(\tau_a/\tau)\right]\right\}^2-\xi^2\right] d\xi d\eta \tag{49}$$

After completing the square in the exponent, Equation (49) becomes

$$\int_{\xi=-\infty}^{\infty} e^{-\xi^2} \int_{\chi=-\infty}^{\xi-2(1-z_n)(\tau_a/\tau)} e^{-\chi^2} d\chi d\xi$$

$$= \int_{\eta=-\infty}^{0} \exp\left\{-\frac{1}{2}\left[\eta-2(1-z_n)(\tau_a/\tau)\right]^2\right\}$$

$$\times \int_{\xi=-\infty}^{\infty} \exp\left(-2\left\{\xi+\left[\eta-2(1-z_n)(\tau_a/\tau)\right]/2\right\}^2\right) d\xi d\eta$$

$$= \sqrt{\frac{\pi}{2}} \int_{\eta=-\infty}^{0} \exp\left\{-\frac{1}{2}\left[\eta-2(1-z_n)(\tau_a/\tau)\right]^2 d\eta\right\}. \tag{50}$$

With the change of variable $v=\left[\eta-2(1-z_n)(\tau_a/\tau)\right]/\sqrt{2}$, we are able to evaluate the remaining integral, so

$$\int_{\xi=-\infty}^{\infty} e^{-\xi^2} \int_{\chi=-\infty}^{\xi-2(1-z_n)(\tau_a/\tau)} e^{-\chi^2} d\chi d\xi$$

$$= \sqrt{\pi} \int_{v=-\infty}^{-\sqrt{2}(1-z_n)(\tau_a/\tau)} e^{-v^2} dv$$

$$= \frac{\pi}{2}\left\{1-\mathrm{erf}\left[\sqrt{2}(1-z_n)(\tau_a/\tau)\right]\right\}. \tag{51}$$

On substituting the values for the three integrals into Equation (47), we obtain our final answer:

$$\left(\frac{dU}{dz}\right)\left(\frac{h}{U_{\mathrm{rad}}}\right) = \frac{3}{U_{\mathrm{rad\,n}}}\left(\frac{1}{z_n} + \frac{1}{2}\sqrt{\frac{\pi}{2}}\left(\frac{\tau}{\tau_a}\right)\left[\frac{1}{z_n^2}+\frac{1}{(1-z_n)^2}\left\{1-\mathrm{erf}\left[\sqrt{2}(1-z_n)(\tau_a/\tau)\right]\right\}\right]\right). \tag{52}$$

The calculation for the energy leaving a unit length of the standing-wave dipole Equation (35) can be performed in a similar manner.

10. References

1. E. K. Miller, "PC's for AP and Other EM Reflections," *IEEE Antennas and Propagation Magazine*, **38**, June 1996, pp. 90-95; **39**, June 1997, pp. 83-89; **40**, February 1998, pp. 96-100; and **42**, August 2000, pp. 87-92.

2. E. K. Miller, "An Exploration of Radiation Physics in Electromagnetics," IEEE International Symposium on Antennas and Propagation *Digest, Volume 3*, Montreal, Canada, July 1997, pp. 2048-2051.

3. G. S. Smith, "On the Interpretation for Radiation from Simple Current Distributions," *IEEE Antennas and Propagation Magazine*, **40**, August 1998, pp. 39-44.

4. R. G. Martin, A. R. Bretones, and S. G. Garcia, "Some Thoughts About Transient Radiation by Straight Thin Wires," *IEEE Antennas and Propagation Magazine*, **41**, June 1999, pp. 24-33.

5. Y. Beers, "The Role of the Larmor Radiation Formula in the Classical Theory of Electromagnetic Radiation," *IEEE Antennas and Propagation Magazine*, **41**, December 1999, pp. 51-55.

6. E. K. Miller and G. J. Burke, "Time-Domain Far-Field Analysis of Radiation Sources," IEEE International Symposium on Antennas and Propagation *Digest, Volume 4*, Salt Lake City, Utah, July 2000, pp. 2058-2061.

7. G. S. Smith, *An Introduction to Classical Electromagnetic Radiation*, New York, Cambridge University Press, 1997.

8. G. S. Smith, "Teaching Antenna Radiation from a Time-Domain Perspective," *American Journal of Physics*, **69**, March 2001, pp. 299-300.

9. M. Abramowitz and I. A. Stegun, *Handbook of Mathematical Functions*, Washington, DC, U. S. Government Printing Office, 1964.

10. T. W. Hertel and G. S. Smith, "The Insulated Antenna – Revisited," *IEEE Transactions on Antennas and Propagation*, **AP-48**, June 2000, pp. 914-920.

Introducing the Feature Article Authors

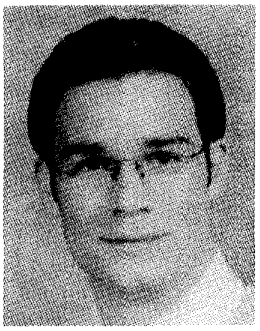

Thorsten W. Hertel was born in Holzminden, Germany, on April 19, 1974. He received the Vordiplom degree in electrical engineering from the Technische Universität Braunschweig, Germany, in 1995, and the MSECE degree from the Georgia Institute of Technology, Atlanta, Georgia, in 1998, where he is currently pursuing the PhD degree in electrical and computer engineering.

His special interests include numerical modeling with the Finite-Difference Time-Domain (FDTD) method and antenna analysis.

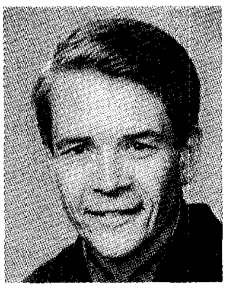

Glenn S. Smith received the BSEE degree from Tufts University, Medford, Massachusetts, in 1967, and the SM and PhD degrees in applied physics from Harvard University, Cambridge, MA, in 1968 and 1972, respectively.

From 1972 to 1975, he served as a Postdoctoral Research Fellow at Harvard University, and also as a part-time Research Associate and Instructor at Northeastern University, Boston, Massachusetts. In 1975, he joined the faculty of the School of Electrical and Computer Engineering at the Georgia Institute of Technology, Atlanta, Georgia, where he is currently Regents' Professor and John Pippin Chair in Electromagnetics.

He is the author of the book *An Introduction to Classical Electromagnetic Radiation* (Cambridge, 1997), and co-author of the book *Antennas in Matter: Fundamentals, Theory and Applications* (MIT Press, 1981). He also authored the chapter "Loop Antennas" in the *Antenna Engineering Handbook* (McGraw-Hill, 1993). He is a member of Tau Beta Pi, Eta Kappa Nu, and Sigma Xi, a Fellow of the IEEE, and a member of USNC/URSI Commissions A and B.

His technical interests include basic electromagnetic theory and measurements, antennas and wave propagation in materials, and the radiation and reception of pulses by antennas.

Editor's Comments *Continued from page 8*

USNC/URSI National Radio Science Meeting. If you are there, please do two things. First, encourage the authors of any papers you hear that you think might make appropriate contributions to the *Magazine* to submit such contributions, either as feature articles or to one of our columns. Second, let me and the other members of our Staff know what we can do to make the *Magazine* more useful and interesting for you. If you're not at the meeting, send in your contributions and your suggestions.

Summer is here, in the northern hemisphere. I'm actually going to try to take some vacation after the Symposium – and perhaps avoid some of the predicted blackouts here in Southern California! I hope that you have a chance over the next few months to pause (at a time of your choosing, with the lights on!), reflect, and perhaps share the results with your colleagues through these pages.

Ross

New IEEE Job Site

A new IEEE Job Web site, at http://www.ieee.org/jobs, features the IEEE e-Recruiter™ job service, which should make the job-hunting process easier and more effective for technical-professional job seekers. The online service, sponsored by IEEE-USA and *IEEE Spectrum*, allows IEEE members worldwide to create and submit a profile of their background and the characteristics they would like in a new job. The service, powered by Hire.com's e-Recruiter software, then scours its extensive database for positions that match what the job hunter has specified. New job postings are continually being added, and the job seeker is notified by e-mail if there is a profile match. The process can be conducted anonymously.

To encourage IEEE members to register and submit their profiles early, *IEEE Spectrum* will award a Personal Digital Assistant to three members who establish a profile within the first 90 days of the site's June 7 launch. The job service is free for IEEE members.

[Information for the above item was taken from an IEEE-USA press release.]

IEEE Master Brand Specifications

The IEEE has decided that its Master Brand shall consist of the IEEE logo (the "kite") and the letters "IEEE" to the right of the kite. The IEEE has established specifications for the IEEE Master Brand, and associated Identity Standards that provide specifications for its use. These are now available at http://www.ieee.org/about/documentation/copyright/IDStandards.pdf on the Web. By adhering to these Standards, the IEEE believes it can enhance the image of the organization and protect ownership of the Master Brand. These Standards include such details as location, color, minimum size, and prominence in use. More information on the use of the IEEE Master Brand is available on the Web at http://www.ieee.org/about/documentation/copyright/ or from Bill Hagen, IEEE Intellectual Property Rights Manager, Tel: +1 (732) 562-3966; E-mail: w.hagen@ieee.org.

Changes of Address

Information regarding subscription addresses is managed by IEEE headquarters. It is *not* maintained, nor can it be changed, by any member of the *Magazine* staff. If you are a member of the IEEE, your subscription is sent to the address in your IEEE member record. To record a change of address, contact IEEE headquarters: Member Address Records, IEEE Headquarters, 445 Hoes Lane, Piscataway NJ 08855-1331 USA; Tel: +1 (908) 981-0060 or +1 (800) 678-4333; Fax: +1 (908) 981-9667; E-mail: address.change@ieee.org. If you are an institutional or other non-member subscriber, contact IEEE Customer Service at the above address, telephone, and fax numbers; E-mail: customer.service@ieee.org. Do *not* send requests to any member of the *Magazine* Staff.